





Frustrated network of indirect exchange paths between tetrahedrally coordinated Co in Ba₂CoO₄

Ifeanyi John Onuorah ^{*}, Muhammad Maikudi Isah , Roberto De Renzi, and Pietro Bonfà 
Department of Mathematical, Physical and Computer Sciences, University of Parma, 43124 Parma, Italy

 (Received 14 May 2021; revised 10 November 2021; accepted 30 November 2021; published 9 December 2021)

We present a detailed study of the electronic and magnetic interactions of Ba₂CoO₄, structurally very uncommon because of the isolated CoO₄ distorted tetrahedral coordination. We show the presence of Co(*d*)-O(*p*) hybridized states characterized by spin polarized oxygen atoms, with their magnetic moments parallel to that on Co. The calculated isotropic exchange interaction parameters, which include the contributions from ligand spins, demonstrate the presence of a three-dimensional (3D) network of magnetic couplings that are partially frustrated in the identified magnetic ground state. Our results indicate that the dominant indirect exchange mechanism responsible for this ground state is mediated by O atoms along the Co–O···O–Co path.

DOI: [10.1103/PhysRevMaterials.5.124407](https://doi.org/10.1103/PhysRevMaterials.5.124407)

I. INTRODUCTION

Cobalt based oxides display unique spin states, electronic properties, and magnetic interactions arising from the nature of the coordinating oxygen atoms and the interaction of the existing multiple degrees of freedom. Ba₂CoO₄ is one of the few known cobalt oxides that exhibits tetrahedral coordination of all Co magnetic ions with a rare case of indirectly linked tetrahedra, as opposed to both the corner and side sharing ones. Indeed, octahedrally coordinated Co has been the subject of more extensive research [1–9] owing to the potential similarities with the cuprate superconductors [10,11]. Conversely, oxides with tetrahedrally coordinated Co are less studied because only but a few are found to be stable in this configuration [12]. Ba₂CoO₄ is one of them, and it offers the opportunity to study the interplay between lattice, charge, and spin degrees of freedom for Co in the tetrahedral environment.

Ba₂CoO₄ crystallizes in a monoclinic lattice structure having space group $P2_1/n$ (No. 14) and lattice parameters $a = 5.9176 \text{ \AA}$, $b = 7.6192$, $c = 10.3970 \text{ \AA}$, and $\beta = 91.734^\circ$ [13]. The unit cell contains four distorted CoO₄ tetrahedra with tetrahedral angles ranging from 104.47° to 112.87° [13]. Each tetrahedron complex is isolated from the other [see Fig. 1(a)], with Co···Co and O···O distances above 4.7 and 3.0 Å, respectively (where ··· indicates the distance between atoms across neighbor tetrahedra). From this geometric inspection, one may expect extremely weak exchange couplings and, as a consequence, very low magnetic transition temperatures. Nonetheless, a surprisingly high Curie-Weiss temperature parameter $|\Theta| \approx 110 \text{ K}$ and antiferromagnetic order below $T_N = 25 \text{ K}$ are observed [13]. To explain the large difference between $|\Theta|$ and T_N , magnetic frustration has been suggested [13,14]. Also, spin dimer analysis with tight binding calculation attributes the origin of the difference in temperature to layered magnetic frustration [14], while an alternative analysis of the spin dynamics with inelastic neutron scattering

[15] and a very recent DFT study [16] assert that quasi-two-dimensional (2D) magnetism could be realized in nonlayered Ba₂CoO₄. Hence, there is the need to fully understand the magnetic interactions together with the nature and origin of the probable indirect exchange interaction that drives magnetism. Also, multiple experimental results establish that the magnetic structure has propagation vector $\mathbf{k} = (0.5, 0, 0.5)$, but the actual alignment of the magnetic moments localized on Co is still debated [15,17–19]. Moreover, the realization of an intermediate spin state for Co was recently proposed to be the cause of the reduced magnetic moment observed experimentally [15]. All these points are indeed open-ended issues that demand further theoretical investigation.

For these reasons we present here a thorough investigation of the electronic properties and magnetic interactions of Ba₂CoO₄ using first-principles calculations. We compare the stability of the proposed magnetic structures, and discuss the roles of oxygen and the isolated distorted tetrahedra in the system. We also calculate the isotropic contribution to the exchange coupling parameters. The obtained values justify many of the magnetic properties highlighted above.

II. METHOD

Ab initio simulations were performed using density functional theory (DFT) within the projector augmented pseudopotentials [20] and the GGA for the exchange correlation functional (Perdew-Burke-Ernzerhof [21]) as implemented in the Quantum Espresso code [22]. We have also considered the role of electron-electron interaction on Co-*d* orbitals by setting the effective Coulomb interaction $U_{\text{eff}} = (U - J)$ value to 5.75 eV, obtained self-consistently in the DFT+*U* scheme [23–27]. The magnetic structure with the experimental propagation vector (0.5, 0, 0.5) was adopted with the use of the $2 \times 1 \times 2$ supercell consisting of 112 atoms. All our calculations were carried out within the collinear spin formalism, although the reported AF magnetic structure is noncollinear with a main component either along the *c* [17] or the *a* axis [15,18,19]. The cutoff used for the plane waves and the charge

^{*}ifeanyijohn.onuorah@unipr.it

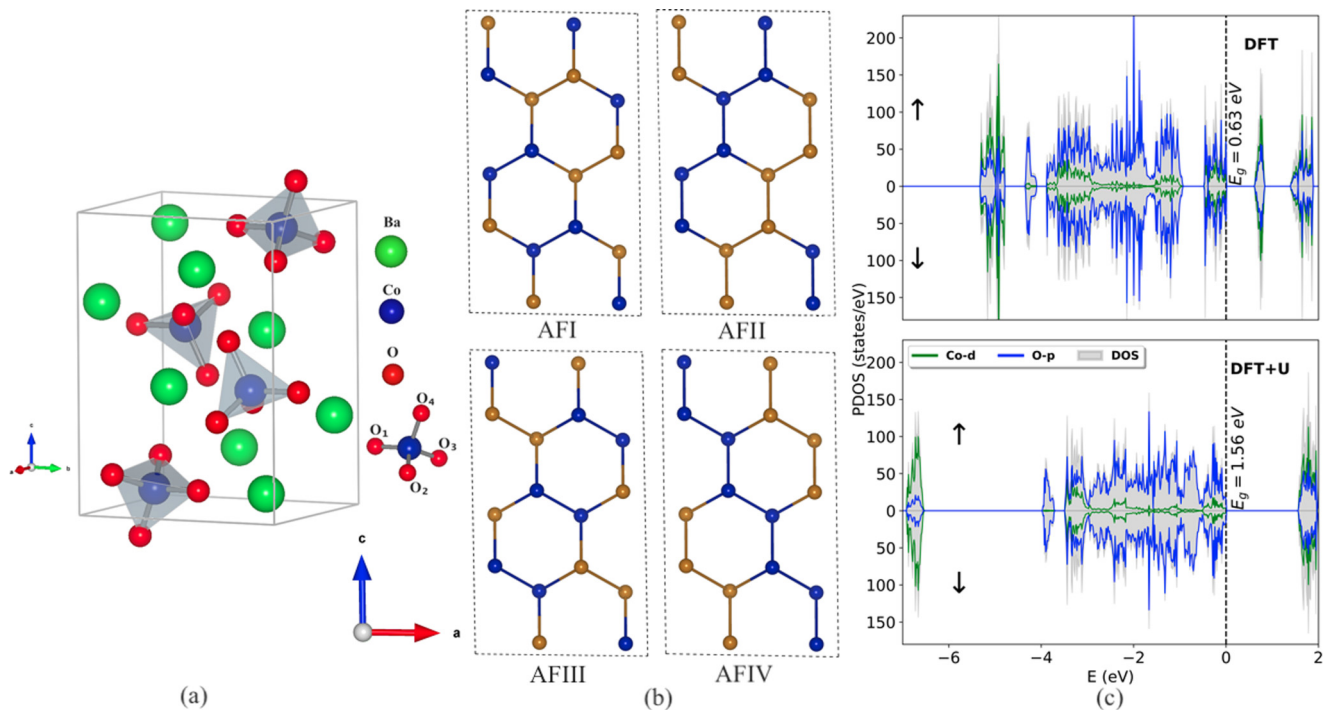


FIG. 1. (a) Unit cell of Ba_2CoO_4 showing the isolated tetrahedral coordination of the Co (blue spheres) and O (red spheres) atoms, the green spheres are the barium atoms. (b) Representation of the four collinear magnetic AF structures considered in the magnetic unit cell. The FM structure is not shown. For clarity, only the Co atoms are shown, color blue for spin up and brown for spin down polarization. Notice that the ac plane is buckled and the plotted Co atoms are not at the same b coordinate. (c) The density of states (gray background) and projected density of states (Co- d and O- p) for both the majority spin (\uparrow) and minority spin (\downarrow) channel of the AFI structure (for DFT and DFT+ U calculations). The zero energy is set to the valence band maximum.

density are 100 and 900 Ry, respectively, with the Brillouin zone sampled using a $3 \times 5 \times 1$ mesh of K points [28]. The Marzari-Vanderbilt [29] smearing with width of 0.005 Ry was used except for the plots and projection of the density of states where the optimized tetrahedron method [30] was adopted. Atomic positions were optimized to force and energy thresholds of 1×10^{-3} a.u and 1×10^{-4} Ry, respectively, while the experimental lattice parameters [13] were adopted. We represented the spin polarized bands in the Wannier function basis [31,32] by projecting onto Co $3d$ and O $2p$ orbitals that span the subspace of 272 Bloch bands.

III. RESULTS AND DISCUSSION

A. Magnetic order

First, we consider the stability of the different magnetic structures. Figure 1(b) shows the four AF magnetic orders in the collinear formalism obtained from the maximal subgroups of the magnetic space groups that allow nonzero magnetic moment on Co, consistent with the experimental propagation vector $(0.5, 0, 0.5)$ [33] (see Table S1 in the Supplemental Material (SM) [34]). Limiting us to the cases with spin polarization along the a or the c axis, the magnetic symmetry distinguishes four collinear AF configurations labeled AFI, AFII, AFIII, and AFIV structures. Notably, several of the quoted experiments [15,17–19] report different magnetic structures (noncollinear versions of AF structures reported above). Additionally, we considered the ferromagnetic struc-

ture labeled FM and the other AF structures discussed in Sec. I of the SM [34], all having higher energies.

Table I shows that our DFT+ U (DFT) results for the AFI structure at the relaxed atomic positions have the lowest energy with respect to the AFII, AFIII, AFIV, and FM structures, separated by 0.208 (2.164), 1.640 (4.744), 3.830 (8.365), and 32.169 (44.428) meV/f.u. respectively. The *very* small energy differences between the AF structures suggest that the magnetic order results from the competition of the various magnetic interactions present in the system.

Table I also shows that, for all these structures, both DFT+ U and DFT determination of the magnetic moment values on each Co remain in good agreement with experimental

TABLE I. Total energy differences with respect to AFI are presented for both DFT+ U and DFT optimized atomic positions in meV/f.u. The moments on Co (obtained from the projection on Co atomic orbitals) for the four AF structures and the FM structure described in the text are presented.

Structure	$\Delta E^{\text{DFT}+U}$ (meV/f.u.)	ΔE^{DFT} (meV/f.u.)	$m_{\text{Co}}^{\text{DFT}+U}$ (μ_B)	$m_{\text{Co}}^{\text{DFT}}$ (μ_B)
AFI	0.0	0.0	2.87	2.82
AFII	0.21	2.16	2.87	2.82
AFIII	1.64	4.74	2.87	2.82
AFIV	3.83	8.37	2.87	2.82
FM	32.17	44.43	2.88	2.84

TABLE II. Occupancy of the Co- d states and an average representative O state (distorted tetrahedral) obtained with DFT+ U .

Spin state	$d_{x^2-y^2}$	d_{z^2}	d_{xz}	d_{yz}	d_{xy}	Total Co- d	Total O- p ^a
Majority	1.00	1.00	0.99	0.99	0.99	4.97	2.90
Minority	0.61	0.60	0.57	0.36	0.33	2.47	2.51
Total						7.44	5.41

^aFor detailed O occupancies see Table S5 in the SM [34].

values: $2.69(4) \mu_B$ [15], $3.5 \mu_B$ [19], and $3.23 \mu_B$ [17]. In addition, an induced moment of $\approx 0.5 \mu_B$, parallel to that on Co, is found on each O atom. This moment on O is common to all the considered magnetic structures and its value does not change significantly among them. From now on we quote only results related to the AFI ground state structure.

B. Hybridization effects

Figure 1(c) shows the density of states (DOS) and projected density of states (PDOS) with atomic orbital contributions from the Co- d and O- p . The plot shows that the band gap increases from 0.63 eV with DFT to 1.56 eV with DFT+ U , indicating the relevance of electron (Coulomb) correlation in the system. These small band gap values suggest a semiconducting behavior for Ba₂CoO₄. Strong hybridization between Co- d and O- p orbitals is indicated by their large contributions to the PDOS both in the valence and in the conduction states around the Fermi energy [Fig. 1(c)].

This strong hybridization is indeed the cause of the relatively large spin polarization on O. Our results are in agreement with very recent DFT calculations [16] and with a model supported by DFT [35] that reveals how the delocalization of O electrons on the Co sites is a consequence of the kinetic energy optimization.

Table II reports the occupation numbers of the Co- d and O- p levels (more details in Tables S4 and S5 in the SM [34]). Notice that these occupation numbers are independent of the AF structures. From a purely ionic picture, the high spin state of Co⁴⁺ is described as a $e_g^2 t_{2g}^3$ configuration with the maximum value of spin $S = 5/2$. However, the hybridization of Co and O states breaks this simplistic description, and the occupation of Co- d levels is found to be substantially higher, approaching ~ 7.5 electrons (see Table II). As a consequence, the magnetic moment on Co atoms is only about $2.87 \mu_B$. This is actually the result of the predominant localization of extra holes on oxygen sites, as shown in Table II, an effect also responsible for the observed magnetic polarization of $0.5 \mu_B$ on each oxygen. Indeed, each Co in a tetrahedron couples with four ligands that totally contribute ≈ 2 hole states to its d orbitals.

A proper description of magnetism in the presence of this strong p - d hybridization requires the inclusion of the ligand states. The overall magnetic moment of this entity is $\approx 5 \mu_B$ and it behaves as an effective total spin $5/2$, in agreement with susceptibility measurements [13,17,36]. The distortion of the tetrahedron completely lifts the degeneracy of the d levels, albeit with a reduced crystal field splitting, typical of tetrahedral vs octahedral coordination. This results in a fine

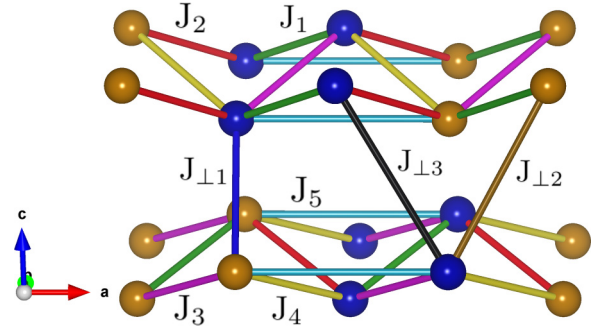


FIG. 2. Magnetic structure of AFI (blue spheres represent \uparrow while brown spheres represent \downarrow on Co) showing the eight exchange couplings considered in this work: five intralayer J_i and three interlayer $J_{\perp i}$. For clarity the couplings are color coded and only one of each is labeled.

adjustment of the fractional occupation of the orbitals, as reported in Tables S4 and S5 of the SM [34].

C. Exchange coupling constants and interaction mechanism

We can now discuss the Co \cdots Co exchange coupling interactions in Ba₂CoO₄ together with the contributions from the induced spin at the ligand sites. The ligand spins, as we have seen, are non-negligible and their effects on the exchange interactions have been discussed in a number of publications on different systems [37–39]. Starting with the Heisenberg Hamiltonian,

$$H = - \sum_{i \neq j} J_{ij} \mathbf{S}_i \cdot \mathbf{S}_j, \quad (1)$$

we treat both the spins on Co and O as localized, where J_{ij} is the isotropic exchange constants between spin \mathbf{S} (normalized to 1) at sites i and j . The isotropic exchange constants were calculated by the Green's function approach [40,41] with the projected Wannier functions as the localized basis.

Starting from the exchange constant contribution from interacting Co pairs $J^{\text{Co}\cdots\text{Co}}$, we use the downfolding procedure by Solovyev [39] as a means to include the effects of the ligand spins (in our case between Co \cdots O and O \cdots O pairs) transferring them to effective coupling interactions between spins at Co sites. This results in the effective exchange constants J^{eff} .

1. Co \cdots Co interaction and ligand spins contribution

Figure 2 shows the spin alignment between Co \cdots Co pairs, which can be described as a layered, buckled structure of dimer chains along the a - b axis, with alternate ordering of the spins in adjacent layers along the c axis. Following the notation used in Ref. [15], we can define two groups of exchange couplings, the intralayer coupling parameters (J_1 , J_2 , J_3 , J_4 , and J_5 , within the ab plane) and the interlayer coupling parameters ($J_{\perp 1}$, $J_{\perp 2}$, and $J_{\perp 3}$, along the c axis).

The calculated exchange coupling constants for both $J^{\text{Co}\cdots\text{Co}}$ and J^{eff} , for distances ranging from 4.76 to 6.07 Å, are reported in Table III. The magnitude of the exchange interactions between pairs of Co atoms farther apart are very small and vanishing relative to the reported values. It

TABLE III. Calculated isotropic exchange constants (in meV) between pairs of Co spins denoted as $J^{\text{Co}\cdots\text{Co}}$ and those including the effects of the ligand spins denoted as J^{eff} obtained with both DFT and DFT+ U . The DFT+ U relaxed distances between two Co ($d_{\text{Co}\cdots\text{Co}}$) (in Å), distances between two O atoms in adjacent tetrahedron ($d_{\text{O}\cdots\text{O}}$) (in Å) and the corresponding Co–O \cdots O, O \cdots O–Co angles (\angle) (in deg) that bridge the Co \cdots Co exchange interactions are shown for each coupling.

	$d_{\text{Co}\cdots\text{Co}}$	$d_{\text{O}\cdots\text{O}}$	\angle	With DFT		With DFT+ U	
				$J^{\text{Co}\cdots\text{Co}}$	J^{eff}	$J^{\text{Co}\cdots\text{Co}}$	J^{eff}
J_1	4.756	3.577	83.15, 83.15	−0.350(1)	−0.149(1)	−0.241(1)	0.024(1)
J_2	4.865	3.245	90.61, 90.61	−0.496(2)	−0.241(3)	−0.337(1)	−0.040(1)
J_3	5.364	3.340	129.92, 114.64	−2.069(6)	−2.941(10)	−1.902(2)	−2.468(3)
J_4	5.461	3.273	137.55, 115.88	−3.031(3)	−4.478(5)	−2.723(3)	−3.654(4)
J_5	5.918	3.004	145.68, 139.09	−2.268(9)	−3.125(14)	−2.334(2)	−3.094(1)
$J_{\perp 1}$	5.192	3.208	119.43, 104.97	−1.219(10)	−1.489(13)	−1.016(1)	−1.032(1)
$J_{\perp 2}$	5.917	3.289	135.40, 115.55	−0.793(1)	−0.983(3)	−0.757(1)	−0.866(1)
$J_{\perp 3}$	6.072	3.304	141.64, 123.41	−0.754(4)	−0.939(6)	−0.719(1)	−0.856(2)

is surprising that J_1 and J_2 have the weakest magnitude of the reported exchange parameters, despite having the shortest Co \cdots Co distances. All the exchange parameters for the Co \cdots Co contribution are antiferromagnetic ($J < 0$) for both DFT and DFT+ U calculations, including J_1 , J_3 , and $J_{\perp 3}$ which couple parallel spins in the AFI magnetic ground state (see Fig. 2).

The magnetic structure is stabilized within the a - b plane by the stronger J_4 and J_5 interactions. A wave vector dependent Heisenberg energy calculation with the DFT+ U exchange constants confirms that the lowest energy state is at the (0.5,0,0.5) propagation vector (see Sec. VI of the SM [34]), in agreement with experimental findings, and that the lowest energy state is AFI, in agreement with collinear DFT+ U and DFT calculations.

The inclusion of the ligand contributions described by the J^{eff} model further weakens J_1 and J_2 and strengthens the other dominant exchange couplings in both DFT and DFT+ U calculations. The above description includes the presence of frustrated antiferromagnetic interactions, as it was previously suggested [14,17]. Indeed, frustration justifies the difference in the mean field estimates of T_N^m and $|\Theta^m|$ that yield $T_N^m = 41.66$ K and $|\Theta^m| = 80.45$ K using $J^{\text{Co}\cdots\text{Co}}$, and $T_N^m = 51.57$ K and $|\Theta^m| = 96.58$ K using J^{eff} in qualitative agreement with the experimental values of $T_N = 25$ K and $|\Theta| = 110$ K (using results from DFT+ U simulations and assuming $S = 5/2$, see Sec. VII of the SM [34] for additional details).

Furthermore, the exchange coupling values reported in Table III show that the interlayer couplings J_{\perp} along the c axis are non-negligible, indicating that the magnetic order has a 3D character, ruling out the earlier reported quasi-2D nature [15]. The fact that J_{\perp} do not vanish is also evidenced by the total energy differences between the AFI and AFII structures which have identical spin alignment within the ab layers but differ in the stacking along c [see Fig. 1(b)].

In addition, treating both Co and O moments as localized spins allows us to also quantify the strong magnetic interaction within each tetrahedron complex. The Co–O couplings are all ferromagnetic with very large values ranging from 48.7 to 59.4 meV. This is due to the strong Co(d)-O(p) hybridization and justifies the intuitive understanding of the tetrahedron magnetic unit, with O spins parallel to that of the central

Co, as an effective moment even in the high temperature paramagnetic regime. This unit has a total moment of $4.88 \mu_B$ obtained by summing the moments from the projection on Co and O atomic orbitals.

2. Exchange mechanism

Let us address the exchange mechanism acting among adjacent CoO $_4$ tetrahedra. The lack of hybridization between

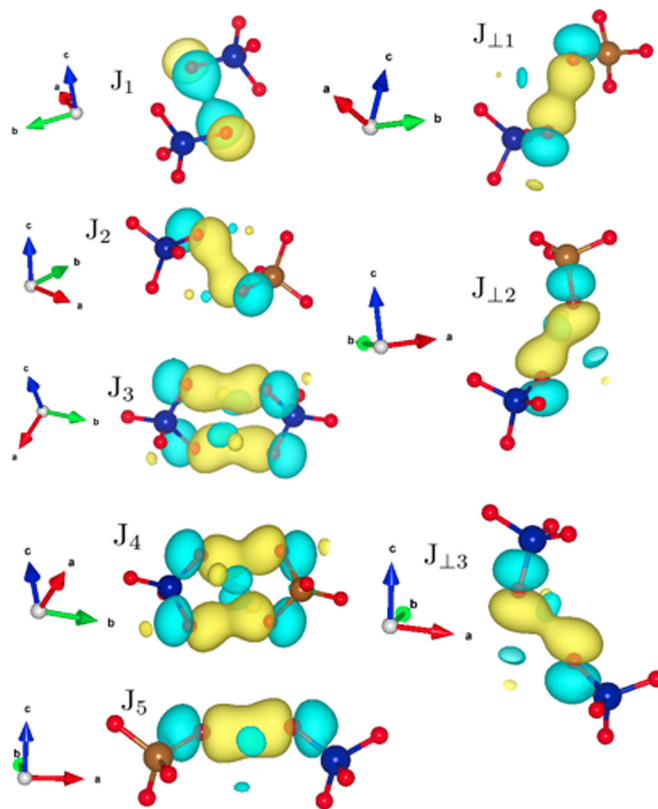


FIG. 3. Isosurface plots of the Wannier functions (spin-up) showing the p orbitals overlap between the O \cdots O atoms along the paths that mediate the exchange interaction between Co in neighbor tetrahedra. Positive isosurface is rendered in yellow and negative in blue, all with the same iso-level.

Ba- p states and O- p or Co- d orbitals makes the contribution of Ba to exchange interactions negligible, even though Co–O...Ba...O–Co is the shortest path between adjacent Co atoms [42]. Unsurprisingly, the inclusion of Ba- p states in the Wannier function basis does not modify the calculated exchange couplings.

The Wannier 3d orbitals centered at the Co sites have large “tails” spreading to the coordinating oxygen sites (see SM [34] Fig. S4) suggesting a more significant role of oxygen in the exchange interaction. The exchange mechanism is clarified with an alternative Wannier basis that includes only the Co- d orbitals, neglecting the O- p orbitals, which results in vanishing values for the coupling parameters. These considerations support the view that exchange interaction via the Co–O...O–Co path dominates the intersite magnetic interactions.

Indeed, a substantial overlap is found between oxygen orbitals of adjacent tetrahedron complexes, as shown in Fig 3. The O...O distances and O...O–Co angles of the bonds that mediate the exchange interaction for each of the Co...Co exchange interaction paths are listed in Table III. The shortest Co...Co distances correspond to the weakest couplings J_1 , J_2 . Qualitatively, this is due to the fact that the O...O distance along these paths are the largest and the angles closest to 90°. Table III shows that for these two weaker couplings the difference between the $J^{\text{Co}\cdots\text{Co}}$ and J^{eff} calculations, neglecting and including the O contribution, respectively, is small, on the order of 0.2 meV, suggesting that the specific presence of a moment on O does not alter drastically the picture of the magnetic interaction, which is already captured by $J^{\text{Co}\cdots\text{Co}}$. This is true also for the other couplings, where the relative difference between the J^{eff} and $J^{\text{Co}\cdots\text{Co}}$ calculations never exceeds 32%.

IV. CONCLUSIONS

In summary, using spin polarized DFT and DFT+ U calculations we have determined the arrangement of magnetic moments in the crystallographic unit cell and we identified the important roles played by O anions in the structurally rare Ba₂CoO₄, where the interesting ground state properties result from the effects of the Co(d)-O(p) hybridized states. We find that the oxygen-hole ligand contributions supersede the original debate on Co spin state, since the bound ligand holes account for the substantially reduced moment observed on Co. The d level states are characterized by a broken tetrahedral symmetry which is observed in our DFT results by distorted Co–O bonds. The calculated exchange coupling constants reveal the 3D nature of the magnetic ordering and show that the not so large difference between the Néel and Curie-Weiss temperatures can be attributed to residual frustration. Therefore, our results show that the complex magnetic behavior of Ba₂CoO₄ is a consequence of the surprisingly strong but frustrated interaction between CoO₄ tetrahedra mediated by O- p orbitals.

ACKNOWLEDGMENTS

We thank Giuseppe Allodi and Paolo Santini for insightful discussions. We acknowledge funding from the SUPER (Supercomputing Unified Platform - Emilia-Romagna) regional project. We also acknowledge computing resources provided by CINECA under Project ID IsC58 and SUPER, the STFC scientific computing department’s SCARF cluster and the HPC resources at the University of Parma, Italy.

-
- [1] J. B. Goodenough, *Mater. Res. Bull.* **6**, 967 (1971).
 [2] R. H. Potze, G. A. Sawatzky, and M. Abbate, *Phys. Rev. B* **51**, 11501 (1995).
 [3] M. A. Korotin, S. Y. Ezhov, I. V. Solovyev, V. I. Anisimov, D. I. Khomskii, and G. A. Sawatzky, *Phys. Rev. B* **54**, 5309 (1996).
 [4] C. Felser, K. Yamaura, and R. Cava, *J. Solid State Chem.* **146**, 411 (1999).
 [5] H. Wu, M. W. Haverkort, Z. Hu, D. I. Khomskii, and L. H. Tjeng, *Phys. Rev. Lett.* **95**, 186401 (2005).
 [6] J. Sugiyama, H. Nozaki, Y. Ikeda, K. Mukai, D. Andreica, A. Amato, J. H. Brewer, E. J. Ansaldo, G. D. Morris, T. Takami, and H. Ikuta, *Phys. Rev. Lett.* **96**, 197206 (2006).
 [7] V. Pardo, P. Blaha, R. Laskowski, D. Baldomir, J. Castro, K. Schwarz, and J. E. Arias, *Phys. Rev. B* **76**, 165120 (2007).
 [8] H. Nozaki, M. Janoschek, B. Roessli, J. Sugiyama, L. Keller, J. H. Brewer, E. J. Ansaldo, G. D. Morris, T. Takami, and H. Ikuta, *Phys. Rev. B* **76**, 014402 (2007).
 [9] J. Kuneš, V. Křápek, N. Parragh, G. Sangiovanni, A. Toschi, and A. V. Kozhevnikov, *Phys. Rev. Lett.* **109**, 117206 (2012).
 [10] K. Takada, H. Sakurai, E. Takayama-Muromachi, F. Izumi, R. A. Dilanian, and T. Sasaki, *Nature (London)* **422**, 53 (2003).
 [11] J. Matsuno, Y. Okimoto, Z. Fang, X. Z. Yu, Y. Matsui, N. Nagaosa, M. Kawasaki, and Y. Tokura, *Phys. Rev. Lett.* **93**, 167202 (2004).
 [12] X. Zhang, V. Stevanović, M. d’Avezac, S. Lany, and A. Zunger, *Phys. Rev. B* **86**, 014109 (2012).
 [13] R. Jin, H. Sha, P. G. Khalifah, R. E. Sykora, B. C. Sales, D. Mandrus, and J. Zhang, *Phys. Rev. B* **73**, 174404 (2006).
 [14] H.-J. Koo, K.-S. Lee, and M.-H. Whangbo, *Inorg. Chem.* **45**, 10743 (2006).
 [15] Q. Zhang, G. Cao, F. Ye, H. Cao, M. Matsuda, D. A. Tennant, S. Chi, S. E. Nagler, W. A. Shelton, R. Jin, E. W. Plummer, and J. Zhang, *Phys. Rev. B* **99**, 094416 (2019).
 [16] Y. Zhang, J. Ning, L. Hou, J. Kidd, M. Foley, J. Zhang, R. Jin, J. Sun, and W. Plummer, *J. Phys. Chem. Solids* **150**, 109803 (2021).
 [17] K. Boulahya, M. Parras, J. M. González-Calbet, U. Amador, J. L. Martínez, and M. T. Fernández-Díaz, *Chem. Mater.* **18**, 3898 (2006).
 [18] P. L. Russo, J. Sugiyama, J. H. Brewer, E. J. Ansaldo, S. L. Stubbs, K. H. Chow, R. Jin, H. Sha, and J. Zhang, *Phys. Rev. B* **80**, 104421 (2009).
 [19] G. Ryu, H. Guo, L. Zhao, M. T. Fernández-Díaz, Y. Drees, Z. W. Li, Z. Hu, and A. C. Komarek, *Phys. Status Solidi (RRL)* **13**, 1800537 (2019).
 [20] P. E. Blöchl, *Phys. Rev. B* **50**, 17953 (1994).
 [21] J. P. Perdew, K. Burke, and M. Ernzerhof, *Phys. Rev. Lett.* **77**, 3865 (1996).
 [22] P. Giannozzi, S. Baroni, N. Bonini, M. Calandra, R. Car, C. Cavazzoni, D. Ceresoli, G. L. Chiarotti, M. Cococcioni, I. Dabo, A. Dal Corso, S. de Gironcoli, S. Fabris, G. Fratesi, R. Gebauer, U. Gerstmann, C. Gougoussis, A. Kokalj, M. Lazzeri,

- L. Martin-Samos *et al.*, *J. Phys.: Condens. Matter* **21**, 395502 (2009).
- [23] I. Solovyev, N. Hamada, and K. Terakura, *Phys. Rev. B* **53**, 7158 (1996).
- [24] S. L. Dudarev, G. A. Botton, S. Y. Savrasov, C. J. Humphreys, and A. P. Sutton, *Phys. Rev. B* **57**, 1505 (1998).
- [25] M. Cococcioni and S. de Gironcoli, *Phys. Rev. B* **71**, 035105 (2005).
- [26] H. J. Kulik, M. Cococcioni, D. A. Scherlis, and N. Marzari, *Phys. Rev. Lett.* **97**, 103001 (2006).
- [27] I. Timrov, N. Marzari, and M. Cococcioni, *Phys. Rev. B* **98**, 085127 (2018).
- [28] H. J. Monkhorst and J. D. Pack, *Phys. Rev. B* **13**, 5188 (1976).
- [29] N. Marzari, D. Vanderbilt, A. De Vita, and M. C. Payne, *Phys. Rev. Lett.* **82**, 3296 (1999).
- [30] M. Kawamura, Y. Gohda, and S. Tsuneyuki, *Phys. Rev. B* **89**, 094515 (2014).
- [31] A. A. Mostofi, J. R. Yates, Y.-S. Lee, I. Souza, D. Vanderbilt, and N. Marzari, *Comput. Phys. Commun.* **178**, 685 (2008).
- [32] G. Pizzi, V. Vitale, R. Arita, S. Blügel, F. Freimuth, G. Géranton, M. Gibertini, D. Gresch, C. Johnson, T. Koretsune, J. Ibañez-Azpiroz, H. Lee, J.-M. Lihm, D. Marchand, A. Marrazzo, Y. Mokrousov, J. I. Mustafa, Y. Nohara, Y. Nomura, L. Paulatto *et al.*, *J. Phys.: Condens. Matter* **32**, 165902 (2020).
- [33] J. Perez-Mato, S. Gallego, E. Tasci, L. Elcoro, G. de la Flor, and M. Aroyo, *Annu. Rev. Mater. Res.* **45**, 217 (2015).
- [34] See Supplemental Material at <http://link.aps.org/supplemental/10.1103/PhysRevMaterials.5.124407> for (i) magnetic symmetry and structure optimization, (ii) search for occupation of Co spin states, (iii) projected density of states, (iv) details of Wannier functions and exchange coupling, (v) oxygen spin contribution to the magnetic interaction, (vi) magnetic structure stability with the Heisenberg model, and (vii) mean-field estimation of T_N and Θ , which includes Refs. [43–49].
- [35] L.-F. Lin, N. Kaushal, C. Şen, A. D. Christianson, A. Moreo, and E. Dagotto, *Phys. Rev. B* **103**, 184414 (2021).
- [36] G. Candela, A. Kahn, and T. Negas, *J. Solid State Chem.* **7**, 360 (1973).
- [37] R. Logemann, A. N. Rudenko, M. I. Katsnelson, and A. Kirilyuk, *J. Phys.: Condens. Matter* **29**, 335801 (2017).
- [38] O. Besbes, S. Nikolaev, N. Meskini, and I. Solovyev, *Phys. Rev. B* **99**, 104432 (2019).
- [39] I. V. Solovyev, *Phys. Rev. B* **103**, 104428 (2021).
- [40] D. M. Korotin, V. V. Mazurenko, V. I. Anisimov, and S. V. Streltsov, *Phys. Rev. B* **91**, 224405 (2015).
- [41] X. He, N. Helbig, M. J. Verstraete, and E. Bousquet, *Comput. Phys. Commun.* **264**, 107938 (2021).
- [42] V. M. Katukuri, P. Babkevich, O. Mustonen, H. C. Walker, B. Fåk, S. Vasala, M. Karppinen, H. M. Rønnow, and O. V. Yazyev, *Phys. Rev. Lett.* **124**, 077202 (2020).
- [43] K. Momma and F. Izumi, *J. Appl. Crystallogr.* **44**, 1272 (2011).
- [44] W. Heisenberg, *Z. Phys.* **49**, 619 (1928).
- [45] A. Liechtenstein, M. Katsnelson, V. Antropov, and V. Gubanov, *J. Magn. Magn. Mater.* **67**, 65 (1987).
- [46] V. V. Mazurenko and V. I. Anisimov, *Phys. Rev. B* **71**, 184434 (2005).
- [47] V. V. Mazurenko, S. L. Skornyakov, A. V. Kozhevnikov, F. Mila, and V. I. Anisimov, *Phys. Rev. B* **75**, 224408 (2007).
- [48] Z. V. Pchelkina and I. V. Solovyev, *J. Phys.: Condens. Matter* **27**, 026001 (2014).
- [49] J. Sólyom, *Fundamental of the Physics of Solids* (Springer, Berlin, 2007), Vol. 1, pp. 473–487.